

Communication

Investigation of Potting-Adhesive-Induced Thermal Stress in MEMS Pressure Sensor

Yunfan Zhang ¹, Bowen Li ², Hui Li ^{1,2,*} , Shengnan Shen ^{1,2}, Feng Li ³, Wentao Ni ² and Wan Cao ⁴

¹ The Institute of Technological Sciences, Wuhan University, Wuhan 430072, China; zhang_yunfan@whu.edu.cn (Y.Z.); shen_shengnan@whu.edu.cn (S.S.)

² School of Power and Mechanical Engineering, Wuhan University, Wuhan 430072, China; li_bowen@whu.edu.cn (B.L.); ni_wentao@whu.edu.cn (W.N.)

³ School of Electrical and Electronic Engineering, Wuhan Polytechnic University, Wuhan 430023, China; lifeng20210719@163.com

⁴ Wuhan FineMEMS Inc., Wuhan 430075, China; wcao@finemems.com

* Correspondence: li_hui@whu.edu.cn

Abstract: Thermal stress is one of the main sources of micro-electro-mechanical systems (MEMS) devices error. The Wheatstone bridge is the sensing structure of a typical piezoresistive MEMS pressure sensor. In this study, the thermal stress induced by potting adhesive in MEMS pressure sensor was investigated by experiments, calculated by analytics and analyzed by simulations. An experiment system was used to test the sensor at different air pressures and temperatures. The error becomes greater with the decrease in pressure. A set of novel formulas were proposed to calculate the stress-strain on Wheatstone bridge. The error increases with the temperature deviating from 25 °C. A full-scale geometric model was developed, and finite element simulations were performed, to analyze the effect of the stress on MEMS pressure sensor induced by different temperatures and thicknesses of potting adhesive. Simulation results agree well with the experiments, which indicated that there is a 3.48% to 6.50% output error in 0.35 mm potting adhesive at 150 °C. With the thickness of potting adhesive increasing, the variations of output error of the Wheatstone bridge present an N-shaped curve. The output error meets a maximum of 5.30% in the potting adhesive of 0.95 mm and can be reduced to 2.47%, by increasing the potting adhesive to 2.40 mm.

Keywords: MEMS pressure sensor; potting adhesive; thermal stress; output error



Citation: Zhang, Y.; Li, B.; Li, H.; Shen, S.; Li, F.; Ni, W.; Cao, W.

Investigation of Potting-Adhesive-Induced Thermal Stress in MEMS Pressure Sensor. *Sensors* **2021**, *21*, 2011. <https://doi.org/10.3390/s21062011>

Academic Editor: Stefano Lenzi

Received: 1 February 2021

Accepted: 10 March 2021

Published: 12 March 2021

Publisher's Note: MDPI stays neutral with regard to jurisdictional claims in published maps and institutional affiliations.



Copyright: © 2021 by the authors. Licensee MDPI, Basel, Switzerland. This article is an open access article distributed under the terms and conditions of the Creative Commons Attribution (CC BY) license (<https://creativecommons.org/licenses/by/4.0/>).

1. Introduction

The micro-electro-mechanical systems (MEMS) pressure sensor is the first industrial MEMS device in the world which was micromachined by Honeywell in 1962 [1]. With the development of electronic processing technology, MEMS pressure sensors have been widely used in industrial productions [2], consumer electronics [3] and vehicles [4]. There are many pressure sensor manufacturers, such as Bosch (Germany), Honeywell (USA) and DENSO (Japan) They keep optimizing the processes to improve the accuracy and reduce the error of pressure sensor.

Process residual stress is one of the main factors in the performance of the pressure sensor. Scientists have done a lot of work to reduce residual stress. Some tried to design new structures, to reduce the output error induced by residual stress. Zhang et al. [5] introduced a novel plastic packaging for MEMS pressure sensor which suggested that the adhesive should be chosen for lower thickness and larger Young's modulus to make better stability. Li et al. [6] designed a novel piezoresistive pressure sensor with a four-beams-bossed-membrane structure which could improve both sensitivity and linearity. Wang et al. [7] introduced an acoustic pressure sensor with an integrated vacuum cavity that could measure pressure without an external package. Tran et al. [8] designed a novel MEMS piezoresistive pressure sensor for low-pressure measurements which had four

independent petal membranes. This structure increased the sensitivity and decreased the nonlinearity of the sensor. These novel designs improved the performance of pressure sensor, but the scientists did not study the mechanism of output error. However, there are other scientists who have done works on it. Krondorfer et al. [9] investigated the stress from the package which caused asymmetric bending deformations on the silicon membrane and resulted in an imbalance of the Wheatstone bridge. Marina et al. [10] analyzed the process-induced residual stresses by a virtual prototyping approach, to study the effect of the process parameters, which showed the distribution of residual stresses caused by the adhesive during the curing. Wu et al. [11] investigated the thermal stress on two sets of electronic control units by moiré interferometry. It showed worse accuracy when the sensors were heated. Zhang et al. [12] studied the output error of inertial measurement unit caused by acoustic injection. Tran et al. [13] investigated the effect of temperature on the output of a piezoresistive sensor and concluded that the thermal performance instability is mainly attributable to the effects of temperature, the residual stress due to fabrication and the residual stress due to packaging. Chiou et al. [14] proposed a methodology that can be used to predict the thermal hysteresis and further improve the sensing element design. Lu et al. [15] studied the thermal stress analysis of chip by finite element model with variations of material properties and geometric parameter of adhesive. Xu et al. [16] used the finite element method to predict the performance of a piezoresistive transducer pressure sensor to thermal and pressure environments. Subbiah [17] characterized the influence of thermal stresses in the sensor and produced a final version of the sensor that is stable for operations at high temperature. Zhang et al. [18] studied the influence of material parameters of bonding adhesive on the performance of piezoresistive pressure sensor. With a lower Young's modulus bonding adhesive, there are lower residual stress and smaller zero offset to the sensor. Chou et al. [19] investigated thermal and packing effects on the sensitivity of pressure sensor. There are large differences of thermal stress at different geometry of protection adhesive, and the uneven type is suggested to reduce thermal effect. Andreas et al. [20] studied the time-dependent hysteresis effects of pressure sensor which cause stresses and lead to signal error. A numerical model was developed to reproduce the sensor behaviors and design the properties of adhesive. The previous studies only focus on novel structures and different material parameters of adhesive but fail to reveal the influence of potting adhesive on the thermal-stress-induced output error of Wheatstone bridge in MEMS pressure sensors.

This paper quantitatively studies the thermal stress–strain induced by potting adhesive in MEMS pressure sensor, which was investigated by experiments, calculated by analytics and analyzed by simulations. An experiment system was used to study the output error of the MEMS pressure sensor at working pressures and temperatures. A set of novel formulas were proposed to study the mechanical effects of thermal stress by calculating the stress–strain on Wheatstone bridge. A full-scale geometric model was developed, and finite element simulations were performed, to optimize the potting process parameter by analyzing the output error of the sensor induced by different temperatures and thicknesses of potting adhesive.

2. Experimental Investigation

A typical piezoresistive MEMS pressure sensor was tested to analyze the output voltage error at different air pressures and temperatures. The research object in this paper is shown in Figure 1. It is a pressure sensor (FN-FPT1065, FineMEMS, Wuhan, China) which contains a piezoresistive MEMS pressure chip (MLX90808, Melexis, Tessenderlo, Belgium). It can be used in the environment of -40 to 150 °C and can detect a maximum pressure of 100 kPa. The Wheatstone bridge resistance of MLX90807 is 10 k Ω . The sensor was calibrated at 25 °C and 0 kPa external pressure. The actual output contains both detecting data and error. Figure 1 shows the sensor without an outside package shell. Its dimension is $18.0 \times 11.0 \times 4.5$ mm, which is mainly composed of five parts: shield ring, potting adhesive, MEMS, bonding adhesive and Al_2O_3 substrate. The MEMS is bonded on

the Al_2O_3 substrate by a bonding adhesive. The shield ring is set to surround the MEMS, to keep the potting adhesive which covers the MEMS chip. For better observation, an optical microscope (DM2500, Leica, Germany) was used to take pictures of the Wheatstone bridge, as shown in Figure 2a. The whole structure of the MEMS pressure chip is shown in Figure 2b whose dimension is $3.83 \times 3.83 \times 0.55$ mm. The Wheatstone bridge is shown in Figure 2c, and it is composed of 4 piezoresistive resistances and wires.

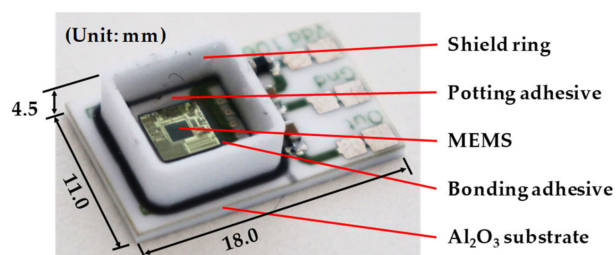


Figure 1. MEMS pressure sensor.

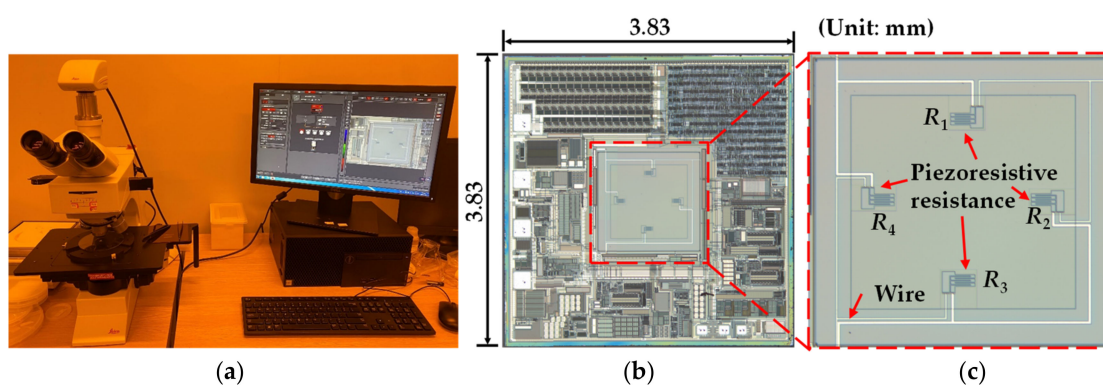


Figure 2. (a) Optical microscope for taking pictures of MEMS pressure chip. (b) MEMS pressure chip. (c) Wheatstone bridge.

The testing system is made of a pressure controller, temperature experiment chamber and electrical instruments (voltmeter, multimeter, etc.), which are shown in Figure 3a. The sensor was tested at different temperatures: -40 , -20 , 10 , 25 , 45 , 65 , 85 , 105 , 115 , 130 and 150 °C. In the meantime, the air pressures loaded on the sensor were changed into 5 , 0 , -20 , -50 , -70 and -95 kPa (the downward pressure is positive, and the upward pressure is negative). A 5 V voltage was supplied to the testing sensor.

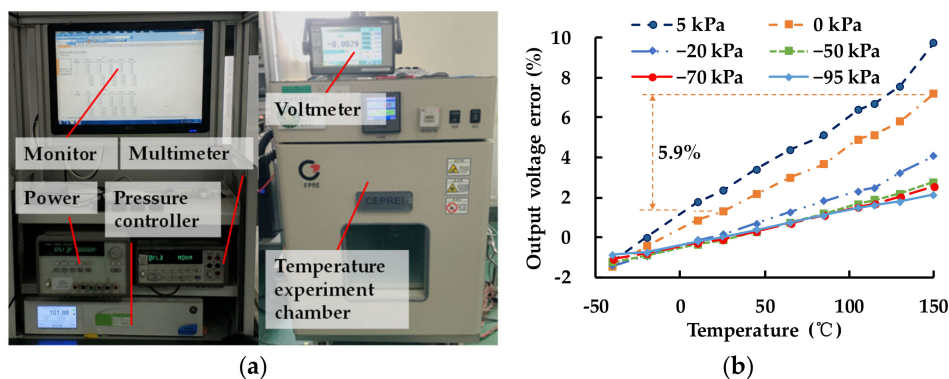


Figure 3. (a) MEMS pressure-sensor testing system; (b) output voltage errors of the MEMS pressure sensor at different air pressures and temperatures.

The output voltage errors of the MEMS pressure sensor are shown in Figure 3b. The sensor was calibrated at 25 °C. It can be found that the output voltage errors become larger

with the temperature increasing. There was a 2.15% maximum error when the sensor was tested from -40 to 150 °C, at the pressure of -95 kPa, a 2.63% error at -70 kPa and a 2.92% error at -50 kPa. When the pressures were lower, the output voltage error got worse. There was a 3.94% error at -20 kPa, 5.90% error at 0 kPa and 7.40% error at 5 kPa. The testing results show that thermal stress has a significant effect on the MEMS pressure sensor and the sensor is more affected under low pressure.

3. Analytic Analysis

Analytic analysis was performed to study output errors of the Wheatstone bridge that are mostly caused by the thermal mismatch between different materials. Figure 4a shows the theoretical model of the MEMS pressure sensor. The structure is simplified into four layers, which respectively correspond to the substrate (Layer 1), bonding adhesive (Layer 2), MEMS chip (Layer 3) and potting adhesive (Layer 4). There are four assumptions in the analytical model: (1) The sensor structure is completely centrosymmetric, to simplify the stress analysis. (2) The material of each layer is homogeneous, isotropic and linearly elastic, to avoid discussing the internal complex stress. (3) The material properties of each layer remain unchanged to simplify the calculation process. Moreover, h_i is the thickness of each layer, h_2' is the thickness of creeping adhesive of Layer 2, b_0 is the width of shield ring and b_1 is the width of center layer. Figure 4b shows the mechanical analysis of Layer 3. There are axial forces caused by horizontal contact layer. F_3^+ is the force on the upper surface, and F_3^- is the force on bottom. F_3' is the level force caused by shield ring, which prevents the expansion of internal structures. Because the Coefficient of Thermal Expansion (CTE) of potting adhesive is larger than other materials, there are vertical forces F_3'' in the side interface between potting adhesive and MEMS chip. F_2 is the vertical force caused by the expansion of Layer 2. As the layer is bent by multiple stresses, there are multiple torques on the Layer 3. M_3 is the anti-clockwise torque caused by horizontal stresses. M_3' is the anti-clockwise torque caused by the creeping part of bonding adhesive. M_3'' is the clockwise torque caused by vertical stresses. The curvature radius of Layer 3 is ρ . The results show the variation of output error of the Wheatstone bridge at different temperatures, which are compared with experiment and simulation results as shown in Figure 9.

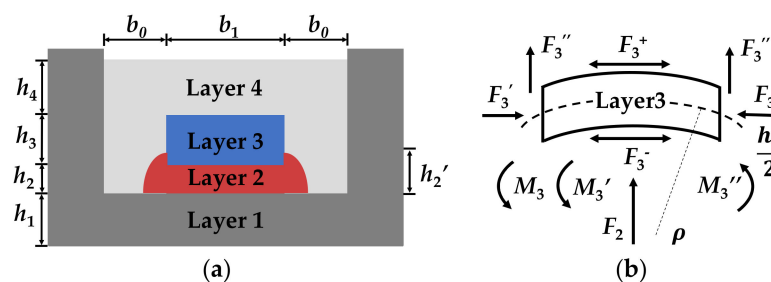


Figure 4. (a) Theoretical model of the MEMS pressure sensor; (b) mechanical analysis of Layer 3.

According to the thermal expansion theory of composite structure, the strains of upper and lower surfaces of the connecting layers are equal in values but opposite in directions. It can be described as follows [21]:

$$\varepsilon_i^+ = \varepsilon_{i+1}^- = \frac{F_i + F_i'}{E_i h_i b_1} + \alpha_i \Delta t + \frac{h_i}{2\rho} = \frac{F_{i+1} + F_{i+1}'}{E_{i+1} h_{i+1} b_1} + \alpha_{i+1} \Delta t - \frac{h_{i+1}}{2\rho} \quad (1 \leq i \leq 3) \quad (1)$$

where ε_i^+ and ε_{i+1}^- are the displacement of upper surface and under surface, respectively; Δt is the difference between loading temperature and room temperature; E_i is the Young's modulus; and α_i is the CTE of each layer. The forces and torques in central structures should be balanced, which leads to the following:

$$\sum_{i=1}^4 F_i \left(\sum_{j=1}^{i-1} h_j + \frac{h_i}{2} \right) + \sum_{i=1}^4 M_i + \sum_{i=2}^3 (M'_i - M''_i) = 0 \quad (2)$$

where M'_i is the anti-clockwise torque caused by the creeping part of bonding adhesive. M''_i is the clockwise torque caused by vertical stresses. M_i , M'_i and M''_i can be calculated as follows:

$$M_i = \frac{E_i h_i^3}{12\rho} \quad (3)$$

$$M'_2 = \frac{E_2 E_4 h_2 \int_0^{h_2} \left[(2\alpha_4 - \alpha_2)(b_0 - \sqrt{h_2'^2 - h^2}) + \alpha_2(b_0 + b_1) \right] \left(\frac{h_2}{2} - h \right) dh \Delta t}{(2E_2 - E_4) \int_0^{h_2} (b_0 - \sqrt{h_2'^2 - h^2}) dh + E_4(b_0 + b_1)h_2} \quad (4)$$

$$M'_3 = \frac{2E_2 E_3 E_4 h_3 \left\{ \int_{h_2}^{h_2'} \left[(\alpha_4 - \alpha_2)(b_0 - \sqrt{h_2'^2 - h^2}) + \alpha_2 b_0 \right] \left(h_2 + \frac{h_3}{2} - h \right) dh + \alpha_3 h_3 b_1 \right\} \Delta t}{2(E_2 E_3 - E_3 E_4) \int_{h_2}^{h_2'} (b_0 - \sqrt{h_2'^2 - h^2}) dh + 2E_3 E_4 b_0 (h_2 - h_2') + E_2 E_4 h_3 b_1} \quad (5)$$

$$M''_2 = \frac{E_2(\alpha_2 - \alpha_4)\Delta t h_2 b_1^2}{4} \quad (6)$$

$$M''_3 = \frac{E_3[(\alpha_4 - \alpha_3), \Delta t(h_2 + h_3 - h_2') + (\alpha_2 - \alpha_3)\Delta t(h_2' - h_2)]b_1^2}{4} \quad (7)$$

where b_1 is the width of the central structure. Then the stress F_3^+ of the upper surface of MEMS can be calculated as follows:

$$F_3^+ = \frac{F_3 + F'_3}{h_3 b_1} + E_3 \alpha_3 \Delta t - \frac{E_3 h_3}{2\rho} \quad (8)$$

4. Numerical Simulation

A full-scale geometric model was developed, and finite element simulations were performed, to analyze the effect of the thermal stress of potting adhesive on the output voltage of the MEMS pressure sensor at different thicknesses of potting adhesive (h_p , the distance of the upper surfaces of MEMS chip and potting adhesive).

4.1. Geometric Model

The geometric model of the MEMS pressure sensor is shown in Figure 5. It is a full-scale model that contains the key structures of shield ring, potting adhesive, MEMS pressure chip, bonding adhesive and Al_2O_3 substrate, as shown in Figure 5a. It has the same geometric data of $18.0 \times 11.0 \times 4.5$ mm with the actual sensor. The MEMS pressure chip is shown in Figure 5b which was simplified by removing the wires and ASIC (Application Specific Integrated Circuit), to reduce the computation cost. Four equivalent piezoresistive resistances are uniformly distributed on the membrane structure with the same orientations. The potting adhesive is designed to cover the MEMS pressure chip, whose h_p is in the range of 0 to 2.8 mm.

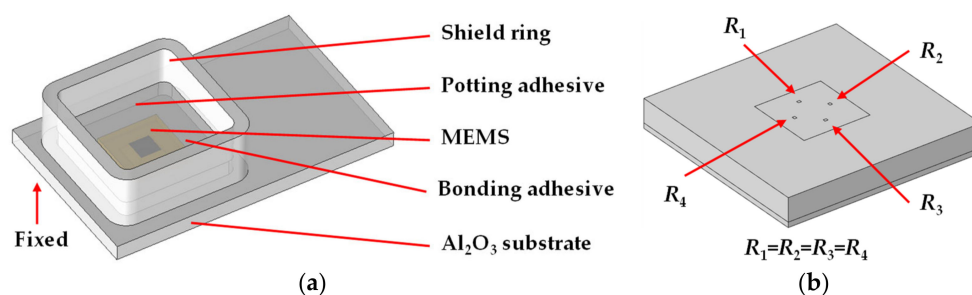


Figure 5. Geometric model of (a) MEMS pressure sensor; (b) MEMS pressure chip.

4.2. Finite Element Model

Figure 6 shows the finite element model of the MEMS pressure sensor. Figure 6a is the general view of the model, and Figure 6b is a magnification of the refined mesh of the MEMS pressure chip. A multi-scale mesh was used in this model, to reduce the computation cost, which contains 197,074 hexahedra and 835,623 tetrahedra elements. The physical properties of CTE (Coefficient of Thermal Expansion), Young's modulus, Poisson's ratio and the density of the MEMS pressure sensor used in the simulation are listed in Table 1. The sensor was fixed at the bottom. The external air pressure applied to the sensor is 0 kPa. The environmental temperature varied from -40 to 150 °C, which is the working temperature range of MEMS pressure sensor. A steady-state solver was used to analyze the stress and strain of MEMS sensor.

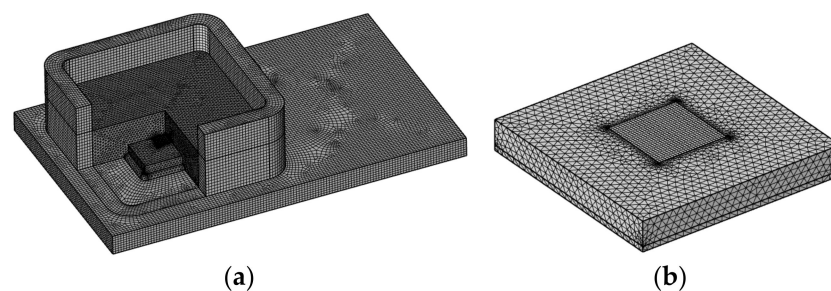


Figure 6. Finite element model of (a) MEMS pressure sensor; (b) MEMS pressure chip.

Table 1. Physical properties of the MEMS pressure sensor.

| Structure | Materials | Property (Unit) | Value | Reference |
|------------------|--------------------------------|-----------------------------|----------------------------------|-----------|
| MEMS | Silicon | CTE (1/K) | 2.6×10^{-6} | [22] |
| | | E (GPa) | 170 | [22] |
| | | μ | 0.28 | [22] |
| | | ρ (kg/m ³) | 2329 | [22] |
| Potting adhesive | Epoxy resin 1 | CTE (1/K) | $(14.9\sim 23.0) \times 10^{-6}$ | [23] |
| | | E (GPa) | 1.30~1.75 | [23] |
| | | μ | 0.3 | [23] |
| | | ρ (kg/m ³) | 2000 | [23] |
| Bonding adhesive | Epoxy resin 2 | CTE (1/K) | $(26\sim 40) \times 10^{-6}$ | [24] |
| | | E (GPa) | 2.2~3.5 | [24] |
| | | μ | 0.3 | [24] |
| | | ρ (kg/m ³) | 1700 | [24] |
| Shield ring | Al ₂ O ₃ | CTE (1/K) | 6.5×10^{-6} | [25] |
| E (GPa) | | 400 | [25] | |
| μ | | 0.22 | [25] | |
| Substrate | | ρ (kg/m ³) | 3965 | [25] |

4.3. Finite Element Simulation

Finite element simulations were carried out by COMSOL 5.5 (COMSOL Inc., Sverige), to study the output error of the MEMS pressure sensor induced by temperature, which varied from -40 to 150 °C. The surface stress displacements of the MEMS pressure chip at different temperatures are shown in Figure 7. It can be found that the thermal stress becomes larger with the temperature increasing from 25 to 150 °C and decreasing from 25 to -40 °C. The stress is mainly concentrated on the areas spliced with the creeping part of bonding adhesive and pressure sensing membrane. The surface strain displacements of the MEMS pressure chip at different temperatures are shown in Figure 8. It can be found that the strain becomes larger with the temperature increasing from 25 to 150 °C, but there is not much strain at low temperatures. The strain is mainly concentrated on the edges of the chip. With the temperature increasing from 25 to 150 °C or decreasing

from 25 to -40 °C, the thermal stress on the surface of the MEMS chip becomes larger. That is the reason of interface thermal mismatch. The MEMS chip is made of silicon, and the potting adhesive is made of organic materials. There are big differences of CTE and Young's modulus between the two materials that lead to thermal stress and strain. The larger the temperature difference, the greater the stress. There are larger stress and strain in the spliced areas with bonding adhesive, which was a result of the larger difference of CTE between bonding adhesive and MEMS chip than potting adhesive and MEMS chip.

The strains of the four piezoresistive resistances of the Wheatstone bridge at different temperatures were obtained and calculated to output errors. The comparison of experiment (Figure 3b), analytics (Equations (1)–(8)) and simulation of the output error at different temperatures at 0 kPa pressure is shown in Figure 9. The simulation results agree well with the experiment results. The FE simulation is based on idea model, but there are many uncontrollable factors in actual processes. The process errors caused by asymmetric bonding, crackle on sensing structure or incomplete package were contained in the results of experiment, making the output error of experiments larger than analytics and simulations. The output error of the MEMS pressure sensor was caused by the imbalance of the Wheatstone bridge. The output error is linearly related to temperature and becomes larger when the temperature deviates from the calibrating temperature of 25 °C.

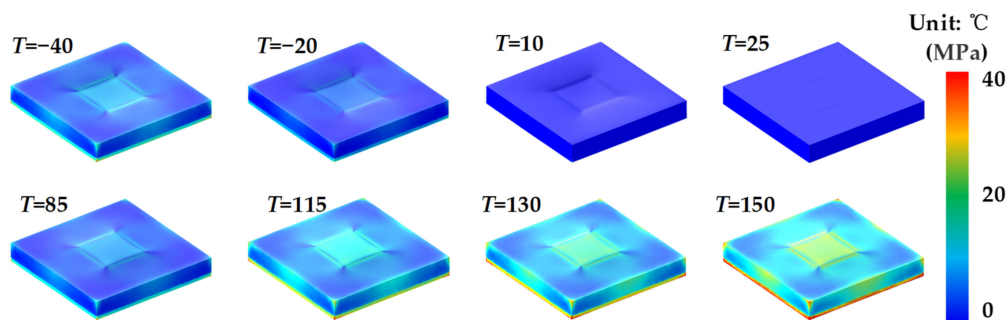


Figure 7. Surface stress of the MEMS pressure chip at different temperatures.

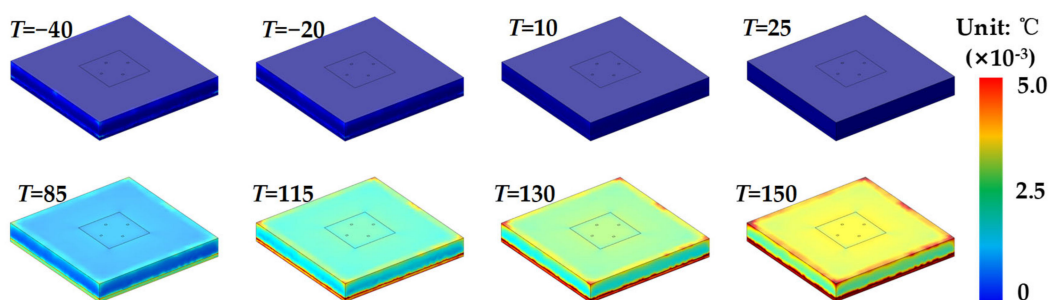


Figure 8. Surface strain of the MEMS pressure chip at different temperatures.

Finite element simulations were carried out, to study the output error of the Wheatstone bridge induced by h_p which varied from 0 to 2.8 mm. The surface stress and strain displacements of the MEMS chip at different h_p are shown in Figures 10 and 11, respectively. It can be found that the stresses of sensing structure are larger than adjacent areas. With the increase of h_p , the stresses of sensing structure increase firstly and then decrease. The strains of the upper surface are relatively similar, which are mainly concentrated on the edges and corners.

The stress of the piezoresistances at different h_p are shown in Figure 12a. The changes of R_1 and R_3 , and R_2 and R_4 are separately described in curves which show “N” shape. It can be found that the stresses grow firstly and reach a maximum of 24.89 MPa (R_1, R_3) and 24.46 MPa (R_2, R_4) when h_p is 0.75 mm. Then the stresses decrease until the h_p comes to 2.20 mm, where the stresses reach a minimum of 21.39 MPa (R_1, R_2, R_3, R_4). At this h_p , the

four piezoresistances in the Wheatstone bridge meet a balance of thermal stress. After that, the stresses grow again with the h_p increase.

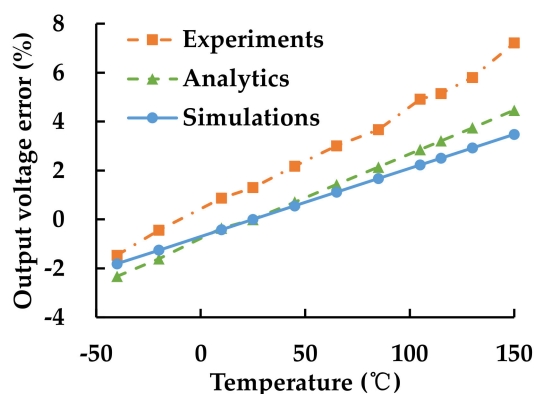


Figure 9. Comparison of the output error of the MEMS pressure sensor, at different temperatures, under 0 kPa pressure.

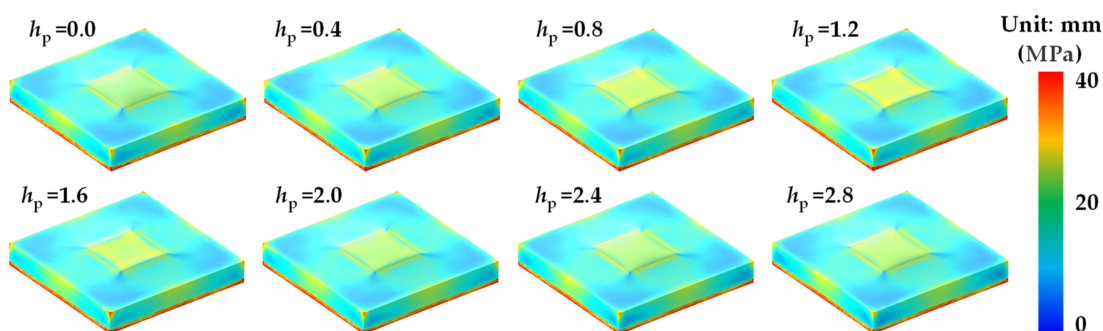


Figure 10. Surface stress of the MEMS pressure chip at different h_p at 150 °C.

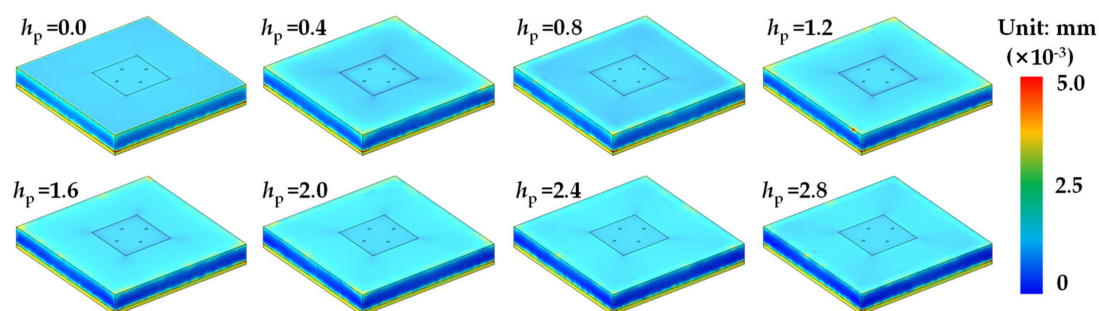


Figure 11. Surface strain of the MEMS pressure chip at different h_p at 150 °C.

The strain of the piezoresistances at different h_p is shown in Figure 12b. The changes of R_1 and R_3 , and R_2 and R_4 are separately described in curves which show an N-shape. It can be found that the strains grow firstly and reach a maximum of 1.903×10^{-3} (R_1, R_3) and 1.893×10^{-3} (R_2, R_4) when h_p is 0.75 mm. Then the strains decrease until the h_p comes to 2.05 mm, where the strains reach the minimum of 1.882×10^{-3} (R_1, R_3) and 1.877×10^{-3} (R_2, R_4). After that, the strains grow again with the h_p increase.

The output errors of the Wheatstone bridge at different h_p are shown in Figure 12c. It can be found that the error grows with the h_p increasing and reaches a maximum of 5.3% when h_p is 0.9 mm. Then the error decreases until the h_p comes to 2.40 mm, where the error is 2.47%. After that, the error grows again with the h_p increase.

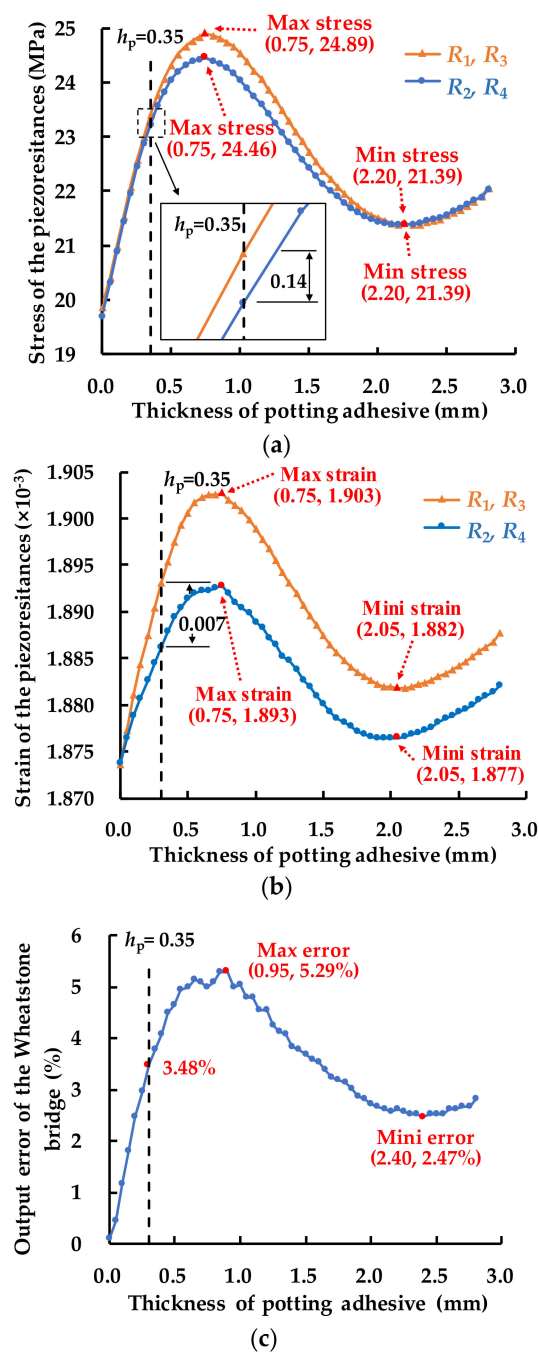


Figure 12. (a) Stress and (b) strain of the piezoresistances at different h_p at 150°C ; (c) output voltage error of the Wheatstone bridge.

It shows a similarity of output error of the Wheatstone bridge in finite element analysis of 3.48% and the thermal stress induced output voltage error in the experiment of 5.90% at the h_p of 1 mm, at the temperature of 150°C . The differences between the two results are due to the other process errors in actual MEMS pressure sensors.

5. Conclusions

In this study, the potting-adhesive-induced thermal stress in the MEMS pressure sensor was investigated by experiments and finite element analysis. Pressure and temperature experiments were conducted, to test the output voltage variation of the MEMS pressure sensor. Thermal–solid coupling finite element simulations were carried out to study the stress–strain of the MEMS pressure chip, as well as the output error of the Wheatstone

bridge. The results between experiments and simulations have a high agreement with each other. It was found that the output error is linearly increasing with the temperature rising or dropping from the calibration temperature. The error varies with the thickness of potting adhesive in an N-shape. The sensor meets the maximum thermal-induced error of 5.29% in the thickness of 0.95 mm and the minimum error of 2.47%, with the thickness increasing to 2.40 mm at 150 °C. This work verifies the feasibility to predict the output error of MEMS pressure sensors by only measuring the thickness of potting adhesive and provides a solution for reducing the output error by strategically adjusting the thickness of the potting adhesive.

Author Contributions: Conceptualization, Y.Z. and H.L.; methodology, Y.Z., H.L. and S.S.; software, Y.Z., W.N., F.L. and B.L.; validation, Y.Z.; formal analysis, Y.Z., H.L. and S.S.; investigation, Y.Z. and W.C.; data curation, Y.Z., W.N. and B.L.; writing—original draft preparation, Y.Z.; writing—review and editing, Y.Z., H.L., F.L. and S.S. All authors have read and agreed to the published version of the manuscript.

Funding: This research was supported by the National Key R&D Program of China, under Grant No. 2019YFB1704600, and the Hubei Provincial Natural Science Foundation of China, under Grant No. 2020CFA032.

Conflicts of Interest: The authors declare no conflict of interest.

References

1. Prosenjit, R. *MEMS and MOEMS Technology and Applications*; SPIE: Bellingham, WA, USA, 2000; ISBN 9780819495983.
2. Cibula, E.; Đonlagić, D. Miniature fiber-optic pressure sensor with a polymer diaphragm. *Appl. Optics* **2005**, *44*, 2736–2744. [[CrossRef](#)] [[PubMed](#)]
3. Ge, G.; Zhang, Y.; Shao, J.; Wang, W.; Si, W.; Huang, W.; Dong, X. Stretchable, transparent, and self-patterned hydrogel-based pressure sensor for human motions detection. *Adv. Funct. Mater.* **2018**, *28*, 1802576. [[CrossRef](#)]
4. Lee, T.H.; Kim, E.S.; Kim, T.H.; Jeong, M.Y. Simple pressure sensor for a vehicle seat using a woven polymer optical-fiber sheet. *J. Korean Phys. Soc.* **2015**, *67*, 1947–1951. [[CrossRef](#)]
5. Zhang, M.; Du, L.; Zhao, Z.; Fang, Z. Low-stress packaging for a MEMS atmosphere pressure sensor. In Proceedings of the IEEE International Conference on Nano/Micro Engineered & Molecular Systems, Suzhou, China, 7–10 April 2013.
6. Li, C.; Cordovilla, F.; Ocaa, J. Design optimization and fabrication of a novel structural piezoresistive pressure sensor for micro-pressure measurement. *Solid State Electron.* **2018**, *139*, 39–47. [[CrossRef](#)]
7. Wang, T.; Tang, Z.; Lin, H.; Zhan, K.; Wan, J.; Wu, S.; Gu, Y.; Luo, W.; Zhang, W. A low temperature drifting acoustic wave pressure sensor with an integrated vacuum cavity for absolute pressure sensing. *Sensors* **2020**, *20*, 1788. [[CrossRef](#)] [[PubMed](#)]
8. Tran, A.; Zhang, X.; Zhu, B. Mechanical structural design of a piezoresistive pressure sensor for low-pressure measurement: A computational analysis by increases in the sensor sensitivity. *Sensors* **2018**, *18*, 2023. [[CrossRef](#)] [[PubMed](#)]
9. Krondorfer, R.; Kim, Y.K.; Kim, J.; Gustafson, C.G.; Lommasson, T.C. Finite element simulation of package stress in transfer molded MEMS pressure sensors. *Microelectron. Reliab.* **2004**, *44*, 1995–2002. [[CrossRef](#)]
10. Marina, S.; Dubravka, R.; Sreco, M. Residual stresses in a pressure-sensor package induced by adhesive material during curing: A case study-ScienceDirect. *Sens. Actuators A Phys.* **2004**, *116*, 442–449.
11. Wu, B.; Kim, D.S.; Han, B.; Palczynska, A.; Gromala, P.J. Thermal deformation analysis of automotive electronic control units subjected to passive and active thermal conditions. In Proceedings of the 16th International Conference on Thermal, Mechanical and Multi-Physics Simulation and Experiments in Microelectronics and Microsystems, Budapest, Hungary, 19–22 April 2015; IEEE: Piscataway, NJ, USA, 2015; pp. 1–6.
12. Zhang, Y.; Li, H.; Shen, S.; Zhang, G.; Yang, Y.; Liu, Z.; Xie, Q.; Gao, C.; Zhang, P.; Zhao, W. Investigation of acoustic injection on the MPU6050 accelerometer. *Sensors* **2019**, *19*, 3083. [[CrossRef](#)] [[PubMed](#)]
13. Tran, A.; Zhang, X.; Zhu, B. Effects of temperature and residual stresses on the output characteristics of a piezoresistive pressure sensor. *IEEE Access* **2019**, *7*, 27668–27676. [[CrossRef](#)]
14. Chiou, J.; Chen, S. Thermal hysteresis analysis of MEMS pressure sensors. *ASME Int. Mech. Eng. Congr. Expo.* **2004**, 47071, 281–288.
15. Lu, C.; Yeh, M. Thermal stress analysis of chip with pressure sensor embedded in accelerometer. In Proceedings of the 2017 International Conference on Electronics Packaging (ICEP), Yamagata, Japan, 19–22 April 2017; IEEE: Piscataway, NJ, USA, 2017; pp. 540–543.
16. Song, X.; Liu, S. A performance prediction model for a piezoresistive transducer pressure sensor. In Proceedings of the Fifth International Conference on Electronic Packaging Technology Proceedings, Shanghai, China, 28–30 October 2003; IEEE: Piscataway, NJ, USA, 2003; pp. 30–35.

17. Subbiah, N.; Feng, Q.; Wilde, J.; Bruckner, G. High-temperature pressure sensor package and characterization of thermal stress in the assembly up to 500 °C. In Proceedings of the Electronic Components and Technology Conference (ECTC), Las Vegas, NV, USA, 28–31 May 2019; IEEE: Piscataway, NJ, USA, 2019; pp. 878–883.
18. Zhang, Z.; Wan, Z.; Liu, C.; Cao, G.; Lu, Y.; Liu, S. Effects of adhesive material on the output characteristics of pressure sensor. In Proceedings of the International Conference on Electronic Packaging Technology & High Density Packaging, Xi'an, China, 16–19 August 2010; IEEE: Piscataway, NJ, USA, 2010; pp. 657–660.
19. Chou, T.L.; Chu, C.H.; Lin, C.T.; Chiang, K.N. Sensitivity analysis of packaging effect of silicon-based piezoresistive pressure sensor. *Sens. Actuators A Phys.* **2009**, *152*, 29–38. [[CrossRef](#)]
20. Dörfler, A.; Feiertag, G.; Schmidt, M.; Ruediger, A.; Wagner, U. Numerical optimization of thermally induced hysteresis effects in the packaging of MEMS pressure sensors. *IEEE Sens. J.* **2019**, *19*, 3633–3639. [[CrossRef](#)]
21. *Strain Calculation in MEMS*; Wuhan FineMEMS Inc.: Wuhan, China, 2018.
22. Uses. Available online: <https://www.britannica.com/science/silicon/Uses> (accessed on 11 March 2021).
23. *Physical Properties of Potting Materials for Pressure Sensor*; Wuhan FineMEMS Inc.: Wuhan, China, 2017.
24. *Physical Properties of Bonding Adhesive for Pressure Sensor*; Wuhan FineMEMS Inc.: Wuhan, China, 2016.
25. Alumina—Aluminium Oxide—Al₂O₃—A Refractory Ceramic Oxide. Available online: <https://www.azom.com/properties.aspx?ArticleID=52> (accessed on 11 March 2021).